Advanced Steel Construction – Vol. 20 No. 1 (2024) 60–68
DOI:10.18057/IJASC.2024.20.1.7

STUDY ON MECHANICAL PROPERTIES OF HONEYCOMB REGULAR HEXAGON DAMPER

Xiao-Dong Li * and Shao-Feng Li

College of Civil Engineering, Lanzhou University of Technology, Lanzhou Gansu 730050
** (Corresponding author: E-mail: xdli@lut.edu.cn)*

ABSTRACT

Traditional metal dampers have the advantages of easy processing, convenient production, and good mechanical properties. However, most of the traditional metal dampers are single design, and their application is limited by the size of the dampers. Based on the honeycomb metal damper, a honeycomb regular hexagon metal damper with a free connection is proposed in this paper. Firstly, the failure mechanism, hysteretic curve, skeleton curve, stiffness degradation curve, and energy dissipation curve of the single energy-dissipating supporting member and the triple two-row supporting member were obtained through the low-cycle reciprocating loading test. Then the R-O mechanical model was fitted to the skeleton curve obtained from the test. Then, three kinds of honeycomb regular hexagon dampers were modeled by ABAQUS finite element simulation software, and the finite element simulation results were compared with the test results. The results show that the energy dissipation support in this paper has a good bearing capacity and energy dissipation capacity, and the development trend of simulation results align with the experimental results. The energy dissipation capacity of the energy dissipation support can be improved, and the multi-section yield can be achieved by connecting multiple energy dissipation units.

ARTICLE HISTORY

Received: 25 May 2023
Revised: 18 October 2023
Accepted: 18 November 2023

KEYWORDS

Honeycomb metal damper;
Energy dissipation support;
Seismic performance;
Hysteretic curve;
Finite element simulation;
Skeleton curve

1. Introduction

Previous earthquakes have shown that adjacent buildings are often damaged or collapsed due to collision under the action of earthquakes [1]. This phenomenon can be seen in many earthquake disasters at home and abroad [2-4]. The application of metal dampers in building structures can improve the energy dissipation capacity and seismic performance of buildings [5-6]. Li et al. [7] proposed a "dual function" metal damper set in the actual steel structure building, which proved that the damper could improve the seismic performance of the structure. Wang et al. [8] proposed a corrugated mild steel damper. The pseudo-static test confirmed that the new damper has the best mechanical performance when the steel plate wave angle is 60°, and the thickness of the steel plate is 6 mm. Based on elastoplastic mechanics, Wu et al. [9] proposed a metal damper restoring force model applied to simulate energy dissipation and a damping system. The results show that the new restoring force model can accurately predict the performance of metal dampers under different conditions and has good universality. Guo et al. [10] designed a steel bar damper, carried out a theoretical analysis of the new damper, and studied its mechanical properties through numerical analysis and a low-cycle reciprocating test. Finally, the optimal shape of a single steel bar is obtained, which proves that the damper can achieve full section yield and prevent stress concentration. Mehmet Alpaslan Köroğlu, et al. [11] has shown from experiment of energy dissipation and seismic performance of structures that damper at beam-column joints can be improved. Zhang et al. [12] proposed a new type of U-shaped steel damper self-centering beam-column connection, and the proposed self-centering connection can provide reliable energy dissipation and self-centering ability. Chen et al. [13] used the general finite element software ABAQUS to discuss the hysteretic characteristics of shear plate dampers under axial pressure. In the past few years, scholars have proposed several new steel dampers with high energy consumption capacity, including mild steel plate dampers [14], shape memory alloy dampers [15-16], U-shaped steel damper [17-19], friction damper [20-22].

Most of the dampers in building structures are single dampers and research on interconnecting dampers is rare. In this paper, a kind of metal energy dissipation brace which can be freely connected is proposed so that the application of dampers in building structures is not limited by size. To understand the hysteretic performance and energy dissipation performance of the support, hysteretic performance, stiffness degradation, and energy dissipation analysis of the energy dissipation support were firstly analyzed through the low-cycle reciprocating test, which proved that the energy dissipation support has good working performance. Secondly, the finite element simulation of the damper is carried out by ABAQUS, and the simulation results are compared with the test results to verify the accuracy of the test.

2. Structure and test design of the energy dissipation support device

2.1. Construction of single support unit

The connectable energy dissipation devices developed in this study are referred to as hexagonal honeycomb dampers, which are categorized into three types: foundation, one-way, and two-way. Their advantages include low steel consumption and good energy dissipation performance. The foundation-type support monomer is divided into the main body unit and ear plate. The main body unit is a regular hexagon, primarily used to dissipate seismic energy. The ear plate connects the left and right monomers, increases the contact area between the left and right support main bodies, and improves the energy dissipation capacity. The ear plate was welded to the support body. The upper and lower parts of the support body were provided with a diamond-shaped notch to connect the upper and lower parts of each monomer. The energy dissipation device was improved by changing the upper and lower corners of the primary element to a circular arc and the diamond notch to a welded ear plate to reduce the influence of stress concentration. Considering the in-plane instability of the energy dissipation units and possible multidirectional earthquake action, the bidirectional/unidirectional brace was further improved by changing the primary body of the energy dissipation device to a bidirectional layout. The new damper was integrally cut and welded from a Q235 steel plate, forming the primary energy dissipation section. Bending deformation was expected to occur at each corner of the regular hexagon under load. However, multisection yielding can be formed to enhance the deformation and bearing capacities of the damper. Fig. 1 shows the single energy dissipation unit.

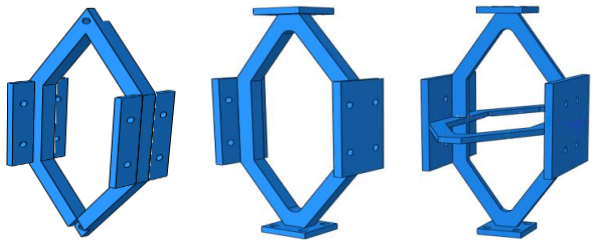

(a) (b) (c)

Fig. 1 3D schematic of each energy dissipation unit type: (a) foundation, (b) one-way, and (c) two-way

2.2. Calculation of individual supporting capacity

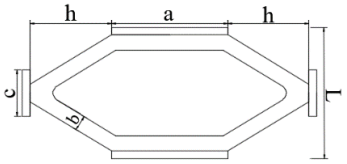

Fig. 2 Single energy dissipation unit dimensions: a-padeye width, b-web width, c-side padeye width, h-energy dissipation section length, and L-energy dissipation unit width

Fig. 2 shows a single energy dissipation unit. According to the elastoplastic mechanics, when a single energy dissipation unit is loaded, the yield and plastic moments at any cross-section of the energy dissipation section can be calculated as follows:

$$M_y = \frac{1}{6}sb^2\sigma_y - \frac{b}{6}F_y, \tag{1}$$

$$M_p = \frac{1}{4}sb^2\sigma_y - \frac{F_{max}^2}{4sb\sigma_y}, \tag{2}$$

where s is the thickness of the energy dissipation section, M_y is the yield bending moment, M_p is the plastic bending moment, σ_y is the yield strength of the material, F_y is the yield bearing capacity of a single energy dissipation unit, and F_{max} is its maximum bearing capacity. F_y and F_{max} can be calculated using Eqs. (3) and (4).

$$F_y = M_y/h \tag{3}$$

$$F_{max} = M_p/h \tag{4}$$

Accordingly, the yield bearing capacity F_y and maximum bearing capacity F_{max} of a single energy dissipation unit can be obtained as follows:

$$F_y = \frac{sb^2\sigma_y}{6h+b}, \tag{5}$$

$$F_{max} = s\sigma_y(\sqrt{4h^2+b^2} - 2h) \tag{6}$$

2.3. Specimen design

Six specimens were designed for the tests. The specimens are denoted by GJ-1, GJ-2, GJ-3, GJ-4, GJ-5, and GJ-6. GJ-1, GJ-3, and GJ-5 are single energy dissipation units. GJ-2, GJ-4, and GJ-6 are energy dissipation supports forming a 3×2 unit using the single energy dissipation units GJ-1, GJ-3, and GJ-5, respectively, which was connected through bolts. The dimensions of the supporting monomers in each component were the same. The bolts used between each support unit were 4.8 grade M4 ordinary hexagonal socket bolts. Fig. 3 shows the primary dimensional parameters and locations of each component (unit/mm).

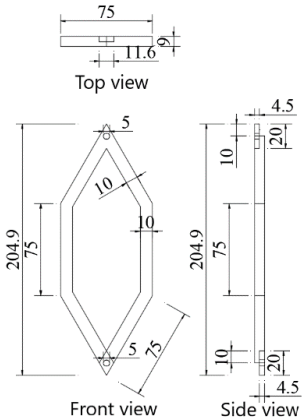

(a) GJ-1

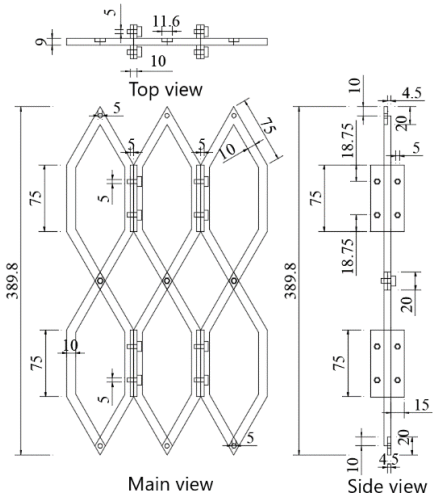

(b) GJ-2

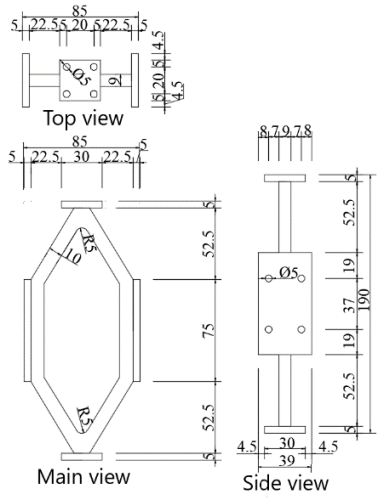

(c) GJ-3

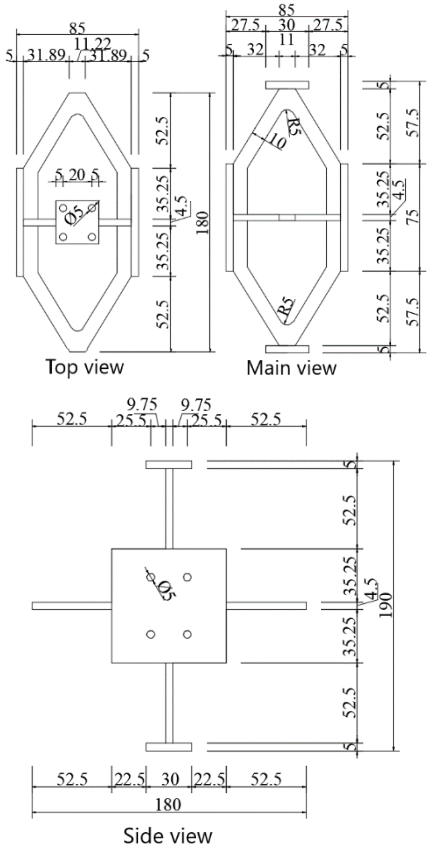

(d) GJ-5

Fig. 3 Geometric dimensions and construction of each test member

2.4. Material property test

The dampers used in this study were made of a 9 mm thick Q235 steel plate. The mechanical properties of the steel plate under uniaxial tension were tested in accordance with the GB/T228.1-2010 Metallic Materials Tensile Testing Part 1: Room Temperature Test Method [23] and completed in the laboratory of the School of Science, Lanzhou University of Technology. Table 1 lists the test results.

Table 1
Mechanical properties of Q235

Sample mark	b (mm)	Fy (Mpa)	Fu (Mpa)	Fy/Fu	δ (%)
1	9	421	576	0.731	20.3
2	9	439	583	0.753	21.2
3	9	434	584	0.743	20.4

Note: b is the width of the sample, Fy is the yield strength of the material, Fu is the tensile strength of the material, Fy/Fu is the material yield ratio, and δ is the elongation after fracture.

2.5. Test equipment and loading system

The test was performed at the Key Laboratory for Disaster Prevention and Reduction of Civil Engineering in Western China and the Civil Engineering Laboratory of Lanzhou University of Technology. A low-cycle reciprocating loading test was performed on the test piece using a microcomputer-controlled electrohydraulic servo single-channel loading device produced by Hangzhou Bangwei Company. The maximum force and displacement of the device were 1000 kN and 200 mm, respectively. The loading methods of test pieces GJ-1, GJ-3, and GJ-5 are as follows: First, two steel plates were used to connect the actuator and base; subsequently, the bolt holes were set at the corresponding positions of the steel plates, and two clips with grooves were used to buckle the test pieces on the upper and lower steel plates. Finally, the steel plates were connected to the grooves of the upper and lower cover plates with bolts. For members GJ-2, GJ-4, and GJ-6, to distribute the force more evenly and simulate the actual working condition of the energy dissipation support device, a 255 mm long steel bar was welded on both sides of the member, and a clip with a groove was added between the two upper and lower support units. Fig. 4 shows the installation diagram of the two components and the loading device diagram. In the test, six members were subjected to displacement loading. The specimen compression was positive, whereas the tension was negative.

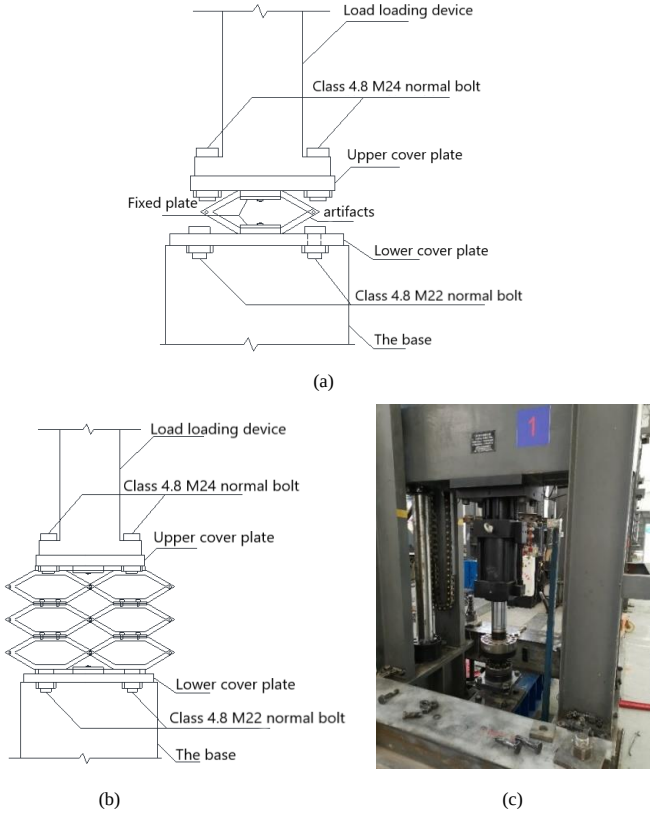

Fig. 4 Mounting diagram of components (a) GJ-1, GJ-3, and GJ-5 and (b) GJ-2, GJ-4, and GJ-6. (c) Schematic of the loading device

The loading displacement at the beginning of the test was 0.5 mm, which increases by 0.5 mm at each stage before reaching 5 mm. After the displacement reached 5 mm, the loading displacement at each level was increased to 1 mm until the component load dropped to 85% of the ultimate load, which was a sign of failure, and the loading was stopped. Fig. 5 shows the loading system and cycle times for each component.

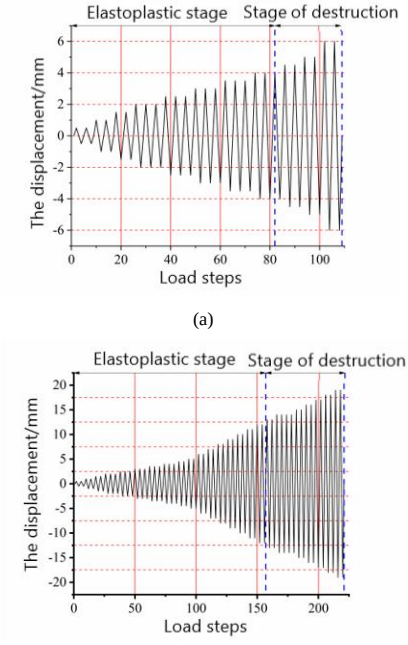

Fig. 5 Loading system of components (a) GJ-1, GJ-3, and GJ-5 and (b) GJ-2, GJ-4, and GJ-6

3. Test results and analysis

3.1. Loading test

In the actual test, owing to the bolt processing problems and improper installation process, some bolts could not achieve the expected connection effect; therefore, some padeye connections were welded to strengthen the connection between the pads without affecting the main body of the energy dissipation support unit. Deformation occurred on the bolt holes at the upper and lower ends of component GJ-1 when the loading displacement amplitude was 3 mm. When the displacement amplitude was 3.5 mm, tiny cracks appeared on the diamond grooves at the upper and lower ends of the component. The cracks on the grooves of the component gradually expanded along the grooves with a continuous increase in displacement. When the displacement was 6 mm, the bearing capacity of the component decreased below 85%, and the loading was stopped. GJ-3 and GJ-5 improved the problem of stress concentration in GJ-1; therefore, the limit displacement was also improved. When GJ-3 was loaded to 8 mm, the short side of the energy dissipation unit arc and the corner of the connection between the energy dissipation unit and padeye almost simultaneously exhibited slight cracks. The cracks gradually expanded with continued loading until they were completely destroyed. The failure mode of GJ-5 was the same as that of GJ-3. Tiny cracks appeared, and the bearing capacity decreased below 85% when GJ-5 was loaded to 9 mm and 14 mm. For member GJ-2, the bolt connection between the energy dissipation elements exhibited relative dislocation when the displacement amplitude was 13 mm. Small cracks appeared at the joints at both ends of the energy dissipation brace, and an expansion trend was observed when the displacement amplitude was 14 mm. When the displacement amplitude was 14–19 mm, cracks appeared at the joints on both sides of the bolted connection between the energy dissipation elements and gradually expanded to the bolt with increased load amplitude. When the load reached 16 mm, the cracks at this location formed a through-crack from the end of the diamond groove to the bolt hole, and the bearing capacity of the component decreased significantly. When the component was loaded to 19 mm, its bearing capacity decreased to less than 85% of the ultimate load, and the test was completed. The failure modes of components GJ-4 and GJ-6 were similar, and a problem of uneven contact surfaces owing to machining errors was encountered. The left and right connecting bolts were staggered when GJ-4 was loaded to 14 mm. After reaching 17 mm, tiny cracks appeared at the ear plate connection of each energy dissipation unit and continued to expand until the component was damaged. The left and right

connecting bolts were staggered when GJ-6 was loaded to 15 mm. Tiny cracks appeared after loading to 18 mm. The component was damaged when GJ-6 was loaded to 21 mm. Fig. 6 shows the cracks and final failure mode of each component.

According to the comprehensive test phenomenon, GJ-1 and GJ-2 weakened this position of the component because the joints were set at both ends of the energy dissipation unit. The joint position of each component had an increasing stress concentration with increasing bearing capacity of the two components. Finally, this position failed before the other positions. GJ-3 and GJ-5 changed the connection mode between the energy dissipation units; there was no stress concentration at the joint, thereby significantly improving the bearing and energy dissipation capacities. Furthermore, GJ-1 and GJ-3 had a tilt degree during crack formation to final failure, whereas GJ-5 had no apparent tilt compared with GJ-1 and GJ-3. Many cracks or failures occurred when GJ-2, GJ-4, and GJ-6 were damaged. Therefore, connecting multiple energy dissipation elements enables multisection failure of members and improves the bearing and energy dissipation capacities.

3.2. Hysteretic behavior

The hysteresis curve of each component had a degree of pinching under tension because the displacement between the component and actuator base was small, and there were errors and defects in the component. This phenomenon was more apparent in the GJ-1 and GJ-2 tests owing to the component processing problem and because the initial error of the actuator was not well adjusted. This phenomenon was significantly improved after subsequent tests. The primary supporting body of each component was inclined, and the bolted connection was unstable during the loading process, resulting in different bearing capacities of the component under tension and compression. This also resulted in an asymmetric hysteretic curve. Figs. 7 and 8 show the corresponding hysteretic properties and skeleton curves for each specimen, respectively. The hysteretic curves of each specimen were approximately shuttle-shaped until the bearing capacity of the damaged member degraded slightly, indicating that the specimen had good energy dissipation and deformation capacities. Table 2 lists the test results for the six test pieces.

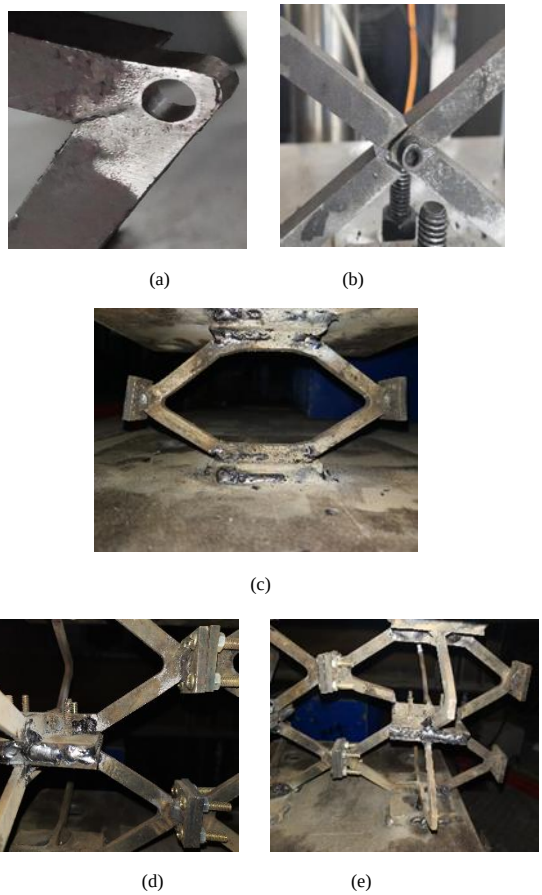

(a) (b) (c) (d) (e)

Fig. 6 Illustrations of different component failures. (a) Cracks appear. (b) Connection starts to break. (c) Crack expands gradually during loading. (d) Cracks appear on multiple sections. (e) Ultimate destruction

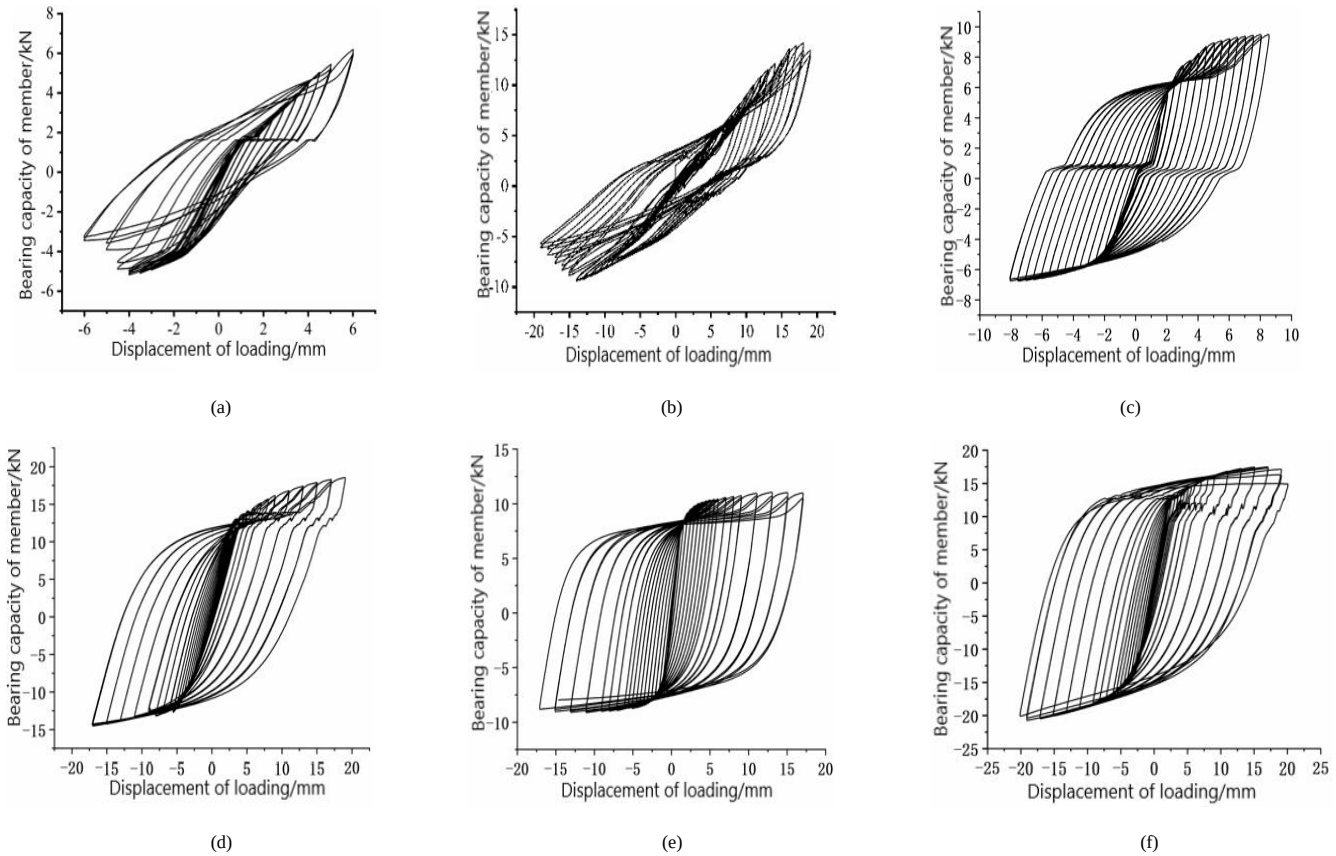

(a) (b) (c) (d) (e) (f)

Fig. 7 Hysteresis curve of components (a) GJ-1, (b) GJ-2, (c) GJ-3, (d) GJ-4, (e) GJ-5, and (f) GJ-6

Table 2
Experiment results of energy dissipation support device

Component No	Loading direction	K_0 (kN/mm)$^{-1}$	Fy/kN	Uy/mm	Fp/kN	Up/mm	Fu/kN	Uu/mm	μ
GJ-1	Negative direction	2.10	2.88	0.88	5.18	4.00	4.40	4.76	5.41
	Forward	1.03	3.02	0.93	6.19	6.00	5.86	7.06	7.59
GJ-2	Negative direction	1.32	3.67	1.54	9.40	14.00	7.99	15.73	10.24
	Forward	1.22	4.53	1.83	14.15	18	13.01	19	10.41
GJ-3	Negative direction	3.54	3.09	0.87	6.52	8.07	5.64	9.33	10.73
	Forward	1.75	3.38	1.12	9.31	8.56	8.82	9.67	8.63
GJ-4	Negative direction	3.39	5.63	1.80	14.32	18.24	12.56	19.56	10.87
	Forward	3.93	6.24	1.77	18.57	18.99	17.23	20.13	11.36
GJ-5	Negative direction	6.71	4.26	1.12	8.82	17.00	7.23	17.63	15.73
	Forward	6.78	5.41	1.14	10.99	17.01	9.16	18.63	16.36
GJ-6	Negative direction	5.71	6.24	1.87	20.08	20.04	19.32	21.42	11.47
	Forward	5.93	5.63	1.76	17.43	20.01	16.46	20.75	11.78

Note: K_0 is the initial stiffness, Fy is the yield load, Uy is the equivalent yield displacement (obtained by geometric method), Fp is the peak load (highest point of the skeleton curve), Up is the peak displacement, Fu is the ultimate load (load when the specimen fails or when the load drops to 85%), Uu is the limit displacement, and μ is the ductility coefficient.

The tensile bearing capacity was less than its corresponding compression bearing capacity when the number of energy dissipation support units increased. The initial stiffness of the members had a downward trend as the number of single members increased. However, the bearing capacity of the members also exhibited a significant increase, primarily because members GJ-2, GJ-4, and GJ-6 were connected by multiple energy dissipation units through bolts compared with members GJ-1, GJ-3, and GJ-5. This decreased the integrity of the component. Thus, the initial stiffness of the components GJ-2, GJ-4, and GJ-6 was relatively smaller than that of a single energy dissipation support element.

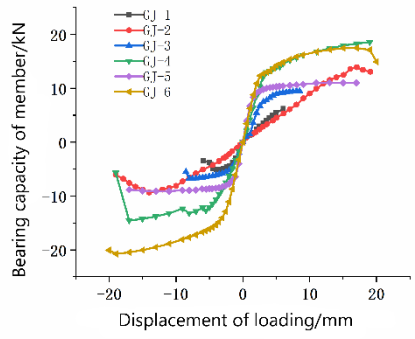

Fig. 8 Skeleton curve of each component

Table 2, Figs. 7(a, c, and e), and Fig. 8 illustrate that the initial stiffness, yield load, and ductility coefficient of GJ-3 and GJ-5 improved compared with those of GJ-1 after changing the connection mode and corners between energy dissipation devices; thus, their energy dissipation and bearing capacities also improved significantly. GJ-5 was plumper and more symmetrical than GJ-1 and GJ-3, indicating that the capacity of the energy dissipation unit can be improved by solving the tilting phenomenon of the supporting body in the loading process.

Table 2, Figs. 7(b, d, and f), and Fig. 8 show that GJ-6 had a fuller hysteretic curve and higher energy dissipation and bearing capacities than GJ-2 and GJ-4. This indicates that the two-way design of GJ-5 can effectively prevent the in-plane displacement of the primary support body and instability of the font caused by connection or loading errors and ensure its energy dissipation and bearing capacities when multiple energy dissipation units are connected.

3.3. Hysteretic behavior

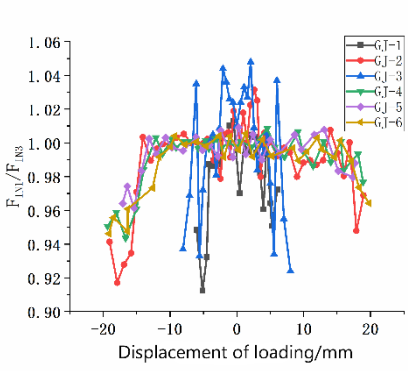

Fig. 9 Bearing capacity degradation curve

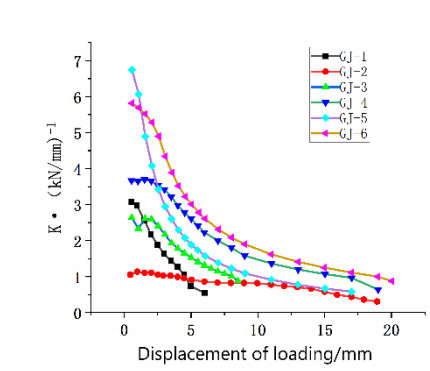

Fig. 10 Stiffness degradation curve

The ratio of the maximum load FIn1 of each stage to the maximum load FIn3 of the second cycle was recorded as the bearing capacity degradation rate to investigate the load-bearing performance of each energy dissipation support device. Under cyclic loading, the equivalent secant stiffness was used to characterize the stiffness of each specimen with a gradual increase in displacement. Figs. 9 and 10 illustrate the bearing capacity and stiffness degradation curves of each member, respectively.

Fig. 9 shows that the degradation of the bearing capacities of different members presents similar change rules: the degradation rate of each member was 0.91–1.04, and the degradation degree of the bearing capacity of each member was small. This indicates that the three single energy dissipation units and the 2×3 units have a good load-bearing capacity.

As shown in Fig. 10, members GJ-1, GJ-3, and GJ-5 are single energy dissipation units with large initial stiffness. The stiffness degradation of a single energy dissipation unit was high, whereas those of the 2×3 units were gradual. Therefore, for members GJ-2, GJ-4, and GJ-6, although their initial stiffness showed a downward trend compared with that of a single energy dissipation unit, their stiffness degradation curves were relatively smooth. This indicates that the stiffness degradation resistance of the energy dissipation support device was better than that of a single energy dissipation element.

3.4. Evaluation of energy dissipation performance of components

The equivalent viscous damping coefficient ξ_e is an important index for evaluating the energy dissipation capacity of structures [24]. Eq. (7) and Fig. 11 show the calculation method for the equivalent viscous damping coefficient. The shaded area in the Fig represents the area of a single hysteresis loop.

$$\xi_e = \frac{1}{2\pi} \cdot \frac{S_{ABC}+S_{CDA}}{S_{OBE}+S_{ODF}} \tag{7}$$

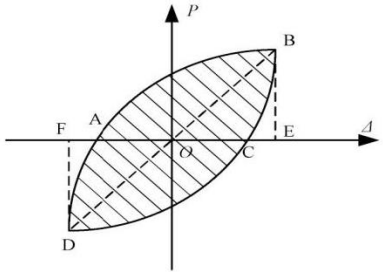

Fig. 11 Schematic of equivalent viscous damping coefficient calculation

This study used the equivalent viscous damping coefficient curve to evaluate the energy dissipation capacity of the energy dissipation braces. As illustrated in Fig. 12, the overall trend of the equivalent viscous damping coefficient of each member increased with an increase in displacement. The equivalent viscous damping coefficient of member GJ-1 did not decrease before failure and reached 0.32, indicating that a single energy dissipation element has a good energy dissipation capacity. The equivalent viscous damping coefficient corresponding to each loading displacement of component GJ-2 fluctuated to varying degrees. A significant fluctuation was observed, particularly when U=1.5–2.5 mm. However, the equivalent viscous damping coefficient of GJ-2 remained above 0.19, reaching a maximum of 0.27. Moreover, the energy dissipation curve of this component exhibited an upward trend. The viscous damping coefficients of members GJ-3, GJ-4, GJ-5, and GJ-6 initially increased rapidly and stabilized between 0.4 and 0.5. The equivalent viscous damping coefficients of each member did not decrease before failure, indicating that the damper has good energy dissipation capacity.

GJ-5 had the largest equivalent viscous damping coefficient, followed by GJ-3, and GJ-1 was the lowest. This indicates that solving the problem of stress concentration and in-plane instability of the energy dissipation element can improve the energy dissipation capacity of the component. The equivalent viscous damping coefficients of members GJ-2, GJ-4, and GJ-6, composed of multiple energy dissipation units, were lower than those of members GJ-1, GJ-3, and GJ-5, composed of their corresponding single energy dissipation units. This indicates that the energy dissipation capacity of the energy dissipation device reduces slightly with an increase in the energy dissipation units.

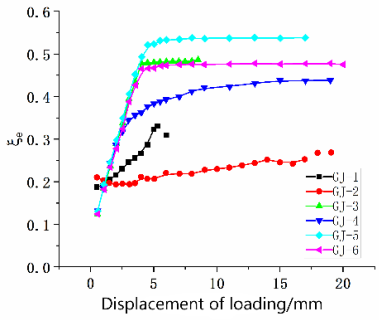

Fig. 12 Comparison of equivalent viscous damping coefficient curves of various components

3.5. Resilience model

This study selected the Ramberg–Osgood (RO) model, which is a continuous curve model, as the restoring force model of the energy dissipation brace to fit the skeleton curve obtained from the test. It has the problem of discontinuous derivatives at individual turning points that the general broken-line model does not have and is more consistent with engineering practice. Moreover, this model requires fewer parameters; therefore, it is a widely used mechanical model. Fig. 13 shows the skeleton curve of the RO model. The skeleton curve is expressed as

$$\frac{U}{U_y} = \frac{F}{F_y}\left(1 + \alpha \left|\frac{F}{F_y}\right|^{\gamma-1}\right), \tag{8}$$

where α and γ are curve shape coefficients; α controls the elastic proportional limit of the curve, and the least square method is used to obtain $\alpha = 0.5$. The control curve represents the stiffness after yielding. $\gamma = 7.1 \cdot ln(t/S) + 29.5$ [25], where t and S are the width and side length of each side of the energy dissipation unit, respectively. When $\gamma = 1$, the curve is completely elastic and plastic. When $\gamma = \infty$, the curve is ideal elastic and plastic. F_y and U_y are the yield load and yield displacement, respectively.

After substituting each loading displacement, the skeleton curve under the RO model can be obtained through calculation, where F_y and U_y denote the yield load and yield displacement in each loading direction, as listed in Table 2. This study fitted only the "rising" segment of the skeleton curve because the RO model does not fit the descending segment. Fig. 14 compares the skeleton curves obtained from the test and calculation of each component.

According to the skeleton curve results calculated using the RO model and those obtained using the test hysteresis curve, the test result of each component in the early stage of loading was more consistent with the RO recovery model. The fitting degree of the two curves decreased with increased loading displacement. However, the RO mechanical model can better fit the energy dissipation brace.

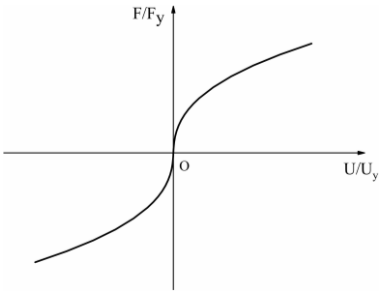

Fig. 13 Ramberg–Osgood (RO) restoration model skeleton curve

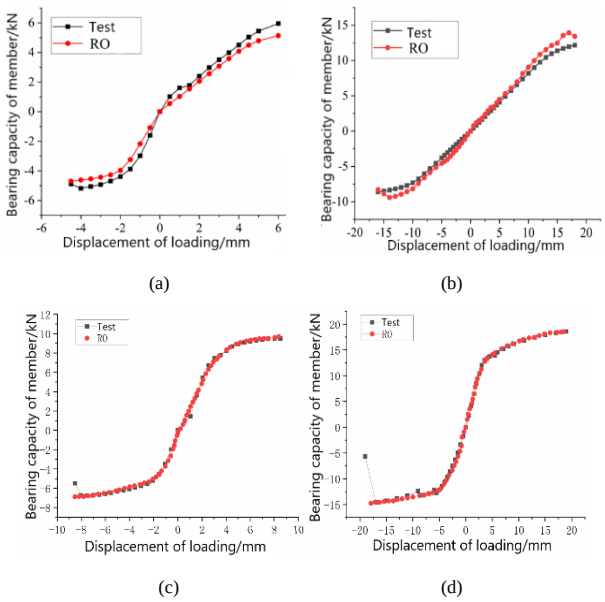

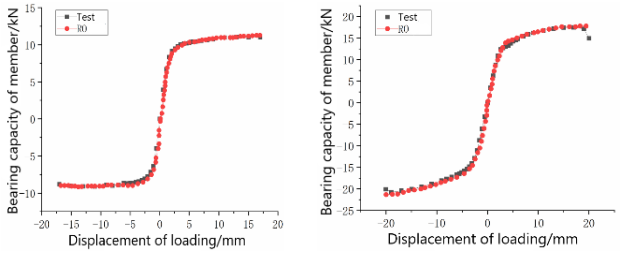

(e) (f)

Fig. 14 Skeleton curve comparison of the RO model and each component test: (a) GJ-1, (b) GJ-2, (c) GJ-3, (d) GJ-4, (e) GJ-5, and (f) GJ-6

4. Finite element simulation analysis of dissipative components

4.1. Basic information of finite element model

By using ABAQUS finite element analysis software, a three-dimensional model was established for three different forms of honeycomb regular hexagon dampers. In the finite element model, honeycomb regular hexagon dampers included energy dissipators and ear plates, whose main function was to make the bearing capacity evenly distributed on the energy dissipators. In addition, eight nodes of linear hexahedron elements were used for the grid division of the finite element model. Furthermore, local mesh refinement was carried out on key research sites, such as around bolt holes and the arc of the honeycomb energy dissipation ring, to observe the failure characteristics of the main body of energy dissipation, which greatly reduced the error of simulation results caused by the grid division of the model. Compared with the test, the factors such as residual stress, initial eccentricity, insufficient welding, and welding heat influence are ignored in the finite element analysis. The finite element analysis ignores the influence of sliding distance and assembly void under low cyclic load. Q235 steel was used in the finite element model of the damper, which was completely consistent with the field test, and Tie binding was used to connect the contact surface. The finite element model and mesh division of the damper is shown in Fig 15.

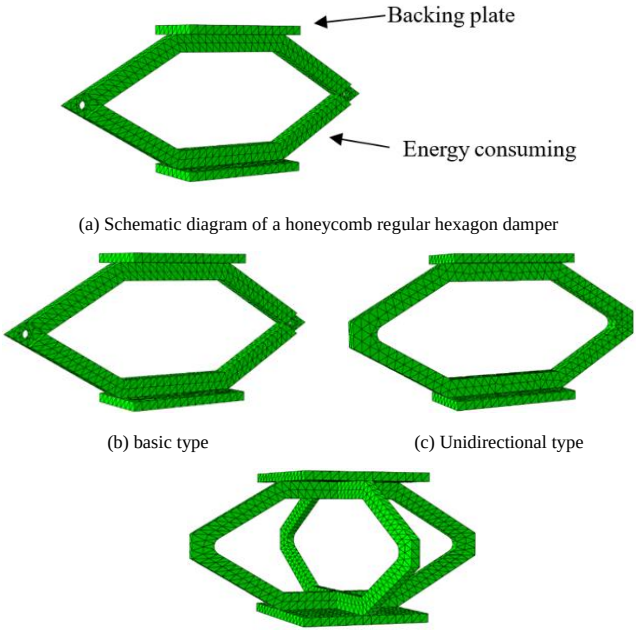

(a) Schematic diagram of a honeycomb regular hexagon damper

(b) basic type (c) Unidirectional type

(d) Bidirectional type

Fig. 15 Finite element model and meshing diagram of a damper

4.2. Finite element model loading conditions and other parameter information

Other parameters of the finite element model are completely consistent with those described in field tests. The basic type of honeycomb regular hexagon damper corresponds to GJ-1, the unidirectional type of honeycomb regular hexagon damper corresponds to GJ-3, and the bidirectional type of honeycomb regular hexagon damper corresponds to GJ-5. In the finite element model, the boundary condition is to simulate the fixed constraint with the six degrees of freedom constraints in the bottom lug plate. To prevent excessive local deformation caused by adverse factors such as stress concentration in the loading process from affecting the simulation results, coupling points were set at the loading position, and displacement loading was carried out on the upper lug plate by coupling constraint mode. The loading mode was cyclic hysteretic loading. The loading process is in complete agreement with the field test. The boundary conditions of the finite element model are shown in Fig 16.

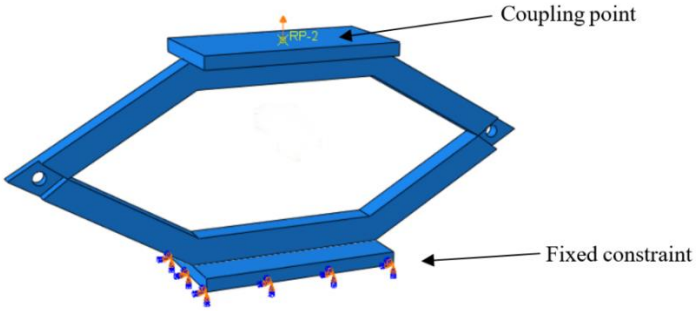

Fig. 16 Boundary conditions of finite element model

4.3. Comparison of failure phenomena

Compared with the honeycomb regular hexagon damper finite element simulation, the failure position of the honeycomb regular hexagon damper test is almost the same as the position of large stress distribution in the finite element model of the damper. However, the phenomenon that the edge of the energy-dissipating body part is separated from the connecting part of the lug plate cannot be simulated in the finite element analysis. Therefore the ductility performance of the two is not completely consistent. But there are other factors of experimental error. In the field test process, there are also some problems, such as uneven connection surface between member and actuator and uneven weld machining, so the field test results are slightly different from the finite element simulation. The comparison between the site failure site of each component and the finite element simulation failure site is shown in Fig 17.

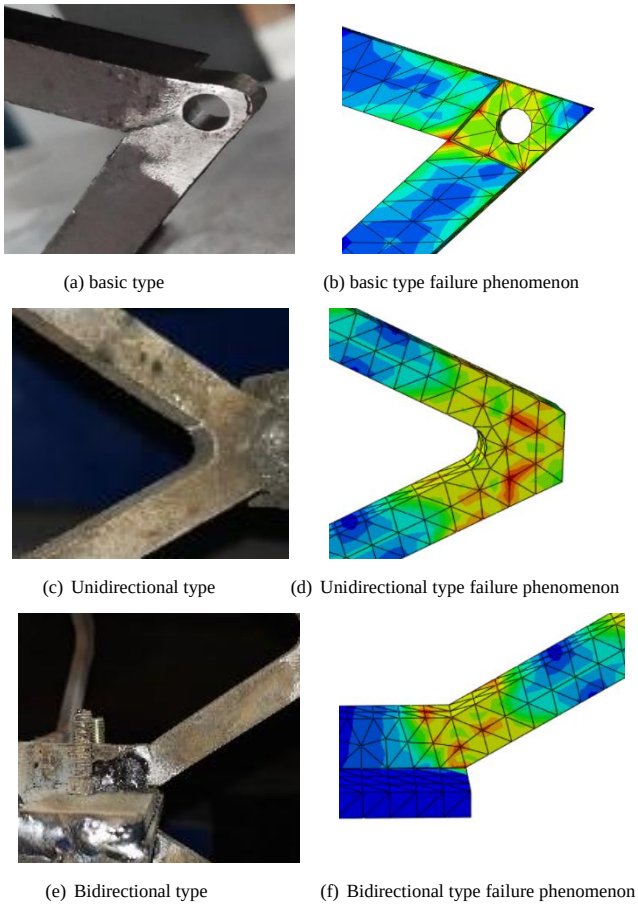

(a) basic type (b) basic type failure phenomenon

(c) Unidirectional type (d) Unidirectional type failure phenomenon

(e) Bidirectional type (f) Bidirectional type failure phenomenon

Fig. 17 Comparison between the site failure phenomenon of each component and the finite element simulation failure phenomenon

As can be seen from FIG. 17, the honeycomb regular hexagon damper foundation first appears to crack at the end of the diamond groove and gradually breaks down. The failure mode of unidirectional and bidirectional honeycomb regular hexagonal dampers is similar, and the stress distribution is large at the arc of the energy-dissipating body, and the angle between the ear plate and the energy-dissipating body, but the stress concentration phenomenon does not appear. The stress distribution in the stress program of the finite element model of the damper is consistent with the failure characteristics of the damper specimen in the field test.

4.4. Comparison of hysteresis curves

As shown in Fig 18 (a), in the comparison between the honeycomb regular hexagon damper basic type field test and finite element test, many unfavorable factors appeared in the field test, such as certain initial displacement errors of the actuator, gap between the damper and the actuator, and uneven welding between the energy dissipation body and the ear plate. The above adverse factors led to the field test did not reach the ideal bearing capacity and a certain degree of pinching phenomenon. In the unidirectional field test of the honeycomb regular hexagon damper, the initial displacement error of the actuator is improved to ensure full contact between the damper and the actuator at the beginning of displacement loading. However, due to the machining problem of the ear plate, the connection between the component and the actuator is uneven, resulting in certain slippage in the displacement loading process, and the bearing capacity is not up to the ideal state. The comparison of the field test and finite element results is shown in Fig 18 (b). In the bidirectional field test of the honeycomb regular hexagon damper, the initial displacement error of the actuator is solved, the contact surface between the damper and the actuator is smooth, and the no-slip phenomenon occurs in the displacement loading process. The hysteresis curve of the field test is fuller and has a higher bearing capacity than that of the foundation type and unidirectional type, but there are some processing problems in the weld between the energy dissipation body and the ear plate. The weld strength is not enough, and there is a certain gap, which makes the field test hysteresis curve under tension and compression asymmetry, and also makes the bearing capacity under tension not reach the ideal bearing capacity. However, the maximum bearing capacity under compression is not much different from the finite element simulation results, and the field test and finite element simulation hysteresis curve trend are the same. The consistency of finite element simulation and field test results is indirectly explained. The comparison of the field test and finite element results of the bidirectional honeycomb regular hexagon damper is shown in Fig 18 (c).

5. Conclusions

The application of dampers in building structures is often limited by their size. Based on the research on the interconnect dampers proposed in this paper. According to the hysteresis curve obtained from the low-cycle reciprocating motion and finite element software model analysis, the following conclusions were drawn:

(1) The damper described in this paper has good hysteretic energy dissipation capacity, especially in the case of large deformation; there is still a full hysteretic loop, and because the damper can be connected, the length is adjustable, so it has good applicability.

(2) According to the bearing capacity degradation curve, stiffness degradation curve, and equivalent viscous damping coefficient curve of components obtained from the low-cycle reciprocating test, it can be seen that the dampers mentioned in the paper all have good load-holding capacity; Among the single dampers GJ-1, GJ-3, and GJ-5, GJ-3, and GJ-5 have the higher bearing capacity and energy dissipation capacity than GJ-1 after solving the problem of stress concentration. Among the three dampers, the hysteretic curves of GJ-5 are fuller and more symmetrical, indicating that the bidirectional design of the support body is conducive to solving the problem of in-plane instability of the energy dissipation member. The three-connection and two-row energy dissipation support test of each energy dissipation unit proves that the connection of multiple energy dissipation units can improve the bearing capacity and energy dissipation performance and can achieve multi-section yield.

(3) The R-O restoring force model based on the damper is also proposed, and the skeleton curve of the damper is simulated. The skeleton curve of the damper can be roughly estimated by the mechanical properties of the material selected by the damper and the size of the energy dissipation support. The comparison with the experimental results shows that the inferred results of this method are reliable.

(4) The yield characteristics of each honeycomb regular hexagon damper are almost identical to those of the large stress part of the stress program in the finite element model of the damper, which fully demonstrates the unity of the finite element simulation results and field test results. According to the hysteretic curve results, the finite element simulation ignored the welding residual deformation and initial defects of the component, as well as the initial error of the actuator and other adverse factors, so there was no slip phenomenon in the finite element simulation results. The energy dissipation laws of the three kinds of dampers in field tests and finite element simulation are the same. The energy dissipation capacity of unidirectional and bidirectional honeycomb regular hexagonal dampers is higher than that of the basic type, while the energy dissipation capacity of the bidirectional type is slightly higher than that of the unidirectional type.

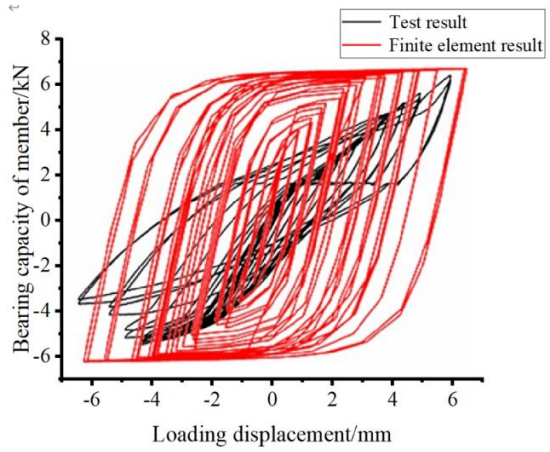

(a) Honeycomb regular hexagonal base type

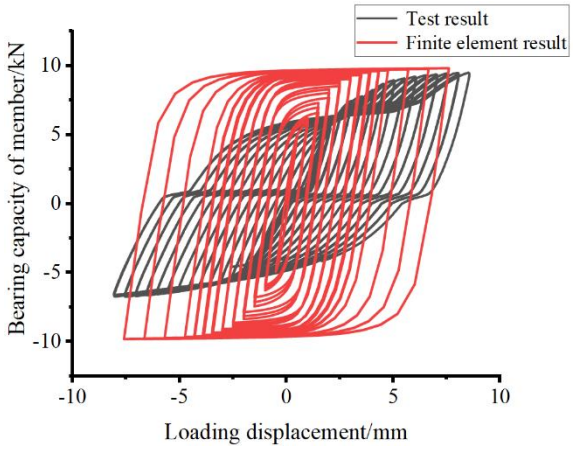

(b) Honeycomb regular hexagonal unidirectional type

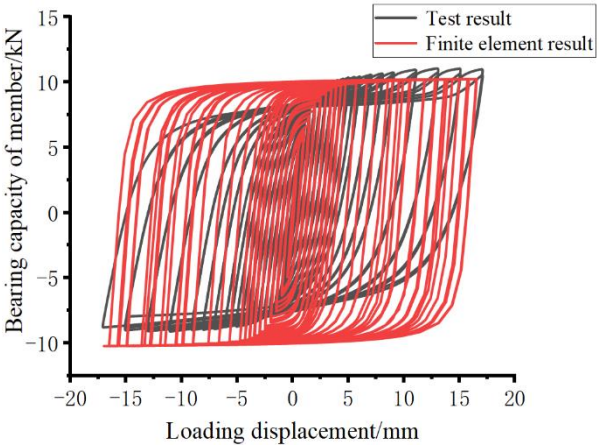

(c) Honeycomb regular hexagonal bidirectional type

Fig. 18 Hysteresis curve comparison

Acknowledgements

We thank the Key Laboratory for Disaster Prevention and Reduction of Civil Engineering in Western China, the Civil Engineering Laboratory of

Lanzhou University of Technology, and the joint efforts of all teachers and students. We would like to thank Editage (www.editage.cn) for English language editing.

Funding: This work was supported by the National Natural Science Foundation of China [grant number 51968043].

References

[1] Y. Zhou, Q. Liang, X. Fang, A review on the earthquake-induced structural pounding, China Civ. Eng. J. 52, 12–22, 2019. (in Chinese).
[2] G. Tselentis, The Athens earthquake of 7 September 1999, Bull. Seismol. Soc. Am. 90, 1143–1160, 2000. https://doi.org/10.1785/0119990168.
[3] G.L. Cole, R.P. Dhakal, F.M. Turner, Building pounding damage observed in the 2011 Christchurch earthquake, Earthquake Engng Struct. Dyn. 41, 893–913, 2012. https://doi.org/10.1002/eqe.1164.
[4] Y. Liu, M. Nishiyama, M. Tani, M. Kurata, K. Iwata, Steel beam with web opening reinforced by induction heating, J. Constr. Steel Res. 176, 106399, 2021. https://doi.org/10.1016/j.jcsr.2020.106399.
[5] V. Gattulli, F. Potenza, U. Di Sabatino, Dissipative coupling for the seismic enhancement of adjacent structures, Eng. Struct. 199, 109520, 2019. https://doi.org/10.1016/j.engstruct.2019.109520.
[6] H. Gokdemir, Failure of horizontal support system to adjacent buildings during reconstruction in Eskisehir, Eng. Fail. Anal. 103 (2019) 82–94. https://doi.org/10.1016/j.engfailanal.2019.04.041.
[7] Li G, Li H N. Experimental study and application in steel structure of ‘dual functions’ metallic damper[J]. Advanced Steel Construction, 9(3), 247-258, 2013.
[8] W. Wang, J. Wang, S.Q. Su, H. Zhang, Y. Liang, Z.-X. Xiang, Experimental research on mechanical behavior of corrugated antisymmetric mild steel damper, J. Build. Struct. 41, 92–100, 2020. (in Chinese).
[9] Wu Zhenhao, Zhuang Liangdong, Huang Yuan. Development and application of a new restoring force model for metallic dampers[J/OL]. China Civil Engineering Journal: 1-12. (In Chinese)
[10] W. Guo, C.-Z. Ma, C. Zeng, Experimental study of a novel steel strip damper, Build. Struct. 48(2), 413–417, 2018. (in Chinese).
[11] Köroğlu M A, Köken A, Dere Y. Use of different shaped steel slit dampers in beam to column connections of steel frames under cycling loading[J]. Advanced Steel Construction, 14(2), 251-273, 2018.
[12] Zhang Y, Li Z, Zhao W, et al. A performance study of beam column connections of self-centering steel frame with U-shaped steel dampers[J]. Advanced Steel Construction, 12(4): 446-465, 2016.
[13] Chen Z, Fan H, Bian G. Parametric analysis of shear panel dampers under high axial compression[J]. Advanced Steel Construction, 11(1): 1-14, 2015.
[14] Teruna D R, Majid T A, Budiono B. Experimental study of hysteretic steel damper for energy dissipation capacity[J]. Advances in Civil Engineering, 2015, 2015: 1-12.
[15] Dutta S C, Majumder R. Shape memory alloy (SMA) as a potential damper in structural vibration control[C]//Advances in Manufacturing Engineering and Materials: Proceedings of the International Conference on Manufacturing Engineering and Materials (ICMEM 2018), 18–22 June, 2018, Nový Smokovec, Slovakia. Springer International Publishing, 2019: 485-492.
[16] Qiu C, Wang H, Liu J, et al. Experimental tests and finite element simulations of a new SMA-steel damper[J]. Smart Materials and Structures, 2020, 29(3): 035016.
[17] Suzuki K, Watanabe A, Saeki E. Development of U-shaped steel damper for seismic isolation system[J]. Nippon Steel Technical Report, 2005, 92: 56-61.
[18] Bagheri S, Barghian M, Saieri F, et al. U-shaped metallic-yielding damper in building structures: Seismic behavior and comparison with a friction dmper[C]//Structures. Elsevier, 2015, 3: 163-171.
[19] Khatibinia M, Jalaipour M, Gharehbaghi S. Shape optimization of U-shaped steel dampers subjected to cyclic loading using an efficient hybrid approach[J]. Engineering Structures, 2019, 197: 108874.
[20] Gagnon L, Morandini M, Ghiringhelli G L. A review of friction damping modeling and testing[J]. Archive of Applied Mechanics, 2020, 90: 107-126.
[21] Monir H S, Zeynali K. A modified friction damper for diagonal bracing of structures[J]. Journal of Constructional Steel Research, 2013, 87: 17-30.
[22] Lee C H, Kim J, Kim D H, et al. Numerical and experimental analysis of combined behavior of shear-type friction damper and non-uniform strip damper for multi-level seismic protection[J]. Engineering Structures, 2016, 114: 75-92.
[23] National Standard of the People’s Republic of China. GB/T 228. 1-2010 Metallic materials-Tensile testing-Part 1: Method of test at room temperature. Beijing: Standards Press of China. 9–19, 2010. (in Chinese).
[24] Y. Chen, T. Liu, H.-J. Jiang, Z.-W. Wan, Experimental study on mechanical properties of annular Q235 steel dampers, J. Build. Struct. 39, 139–147, 2018. (in Chinese).
[25] A. Baird, T. Smith, A. Palermo, et al., Experimental and numerical study of U-shape flexural plate (UFP) dissipaters, in: Technical Conference and AGM, Auckland, NZ, 21–23 March 2014, New Zealand Society for Earthquake Engineering, 2014 paper Number P2.